Spectral features of vibrational Te isotopes

J. B. Gupta ●*

Ramjas College, University of Delhi, Delhi 110007, India

The variation of collective vibrational spectra with varying N displayed by the $Z = 52$ Te isotopes, for less than $N = 82$ closed shell, are of special interest. The spectral features of the ground band and the two and three phonon excited multiplets in $^{118-128}$Te, are studied here empirically. The state energy $E(2_1^+)$ increases, and the energy ratio $R_{4/2}$ decreases with increasing neutron number N. Also the 0_2^+ state rises up sharply, and the 0_3^+ state follows it, unlike their relation in the E(5) symmetry. It is shown that ^{120}Te isotope displays the weakly deformed status, and the heavier isotopes move towards the spherical harmonic vibrator status. The interacting boson model (IBM-1) is used to reproduce these spectral features of $^{118-124}$Te, with use of slight variation of boson energy ε and of the quadrupole interaction strength. In the microscopic approach, the dynamic pairing plus quadrupole model of Kumar and Baranger also reproduces these basic spectral features.

I. INTRODUCTION

The $Z = 52$ ($N < 82$) Te isotopes with one valence proton pair above the $Z = 50$ shell closure display interesting spectral features. Seen vertically up to spin 6^+, the ground bands exhibit almost equally spaced energy levels. The energy ratio $R_{4/2} = E(4_1^+)/E(2_1^+)$ is 2.1 or less, close to the value of 2.0 for the spherical harmonic vibrator. But in some isotopes, the nonvanishing finite $B(E2, 0_1^+ - 2_1^+)$ values and the quadrupole moment $Q(2_1^+)$ have been observed in Coulomb excitation experiments by Barrette *et al.* (1974) [1], Mansi *et al.* (2014) [2], and Mansi *et al.* (2018) [3]. This presents an anomalous feature, and has been the topic of experimental and theoretical studies in the past and in recent years. In the present study, this dichotomy is analyzed by studying the various empirical indicators, and by using the collective models of nuclear structure.

Barrette *et al.* (1974) [1] studied the $A = 122$–130 Te isotopes in the Coulomb excitation experiment. Bockish *et al.* (1976) [4] did the reorientation experiment to determine the quadrupole moment (QM) in $^{122-130}$Te. Robinson, Hamilton, and Snelling (1983) [5] did the directional correlation experiment, to determine the spin and parity of the low lying levels in ^{124}Te, and noted the absence of the $I^\pi = 0^+$ state of the two phonon triplet, and its rise to the $n = 3$ phonon multiplet energy level, which led them to associate its level structure with the O(6) symmetry of the interacting boson model (IBM) [6]. Mansi and co-workers [2,3] did Coulomb excitation experiments to study ^{120,122}Te isotopes and compared their results with the Davydov-Filippov asymmetric rotor model [7] and IBM-2 [6]. Hicks *et al.* (2017) [8] determined the lifetimes of the levels in ^{124}Te. More recently, Hicks *et al.* (2022) [9]

studied $N = 78$ ^{130}Te in the $(n, n' \gamma)$ reaction, and did a large scale shell model calculation.

In the following, first in Sec. II, a brief description of the interacting boson model (IBM-1) [6] for the collective motion and of the microscopic dynamic pairing plus quadrupole (DPPQ) model of Kumar and Baranger [10,11] is given. The empirical features of the ground band and of the two and three phonon excited multiplets are illustrated in Sec. III, to highlight the spectral features of Te isotopes. The model study is limited to the $A = 118$–124 Te isotopes, which display the relatively larger anharmonicity. The data on other isotopes are included in the empirical study, where required. The predicted energy spectra are given in the tables and figures. The $B(E2)$ values and interphonon multiplet $B(E2)$ ratios are compared with the values from theory. The $V(\beta, \gamma = 0)$ and $V(\beta, \gamma)$ plots from the DPPQ model for ^{120}Te are given in Sec. IV. A summary is given in Sec. V.

II. THEORY

A. Interacting boson model (IBM)

The algebraic interacting boson model (IBM) [6] enables the prediction of the eigenvalue spectrum and the $B(E2)$ values of the given nucleus. With the assumption of the conservation of boson number $N_b = N_p + N_n$ in the boson-boson interaction, representing the correlated nucleon pairs (proton and neutrons, valence particles, or holes) one gets the U(6) group, which has 3 dynamical subgroups U(5), SU(3), and O(6). The U(5) group chain is defined as

$$\text{U}(6) \supset \text{U}(5) \supset \text{O}(5) \supset \text{O}(3) \supset \text{O}(2). \quad (1)$$

The four term Hamiltonian $H_{\text{IBM}}-1$ may be written as

$$H_{\text{IBM}} = \varepsilon\, n_d + k\, Q \cdot Q + k'\, L \cdot L + k''\, P \cdot P. \quad (2)$$

---

*jbgupta2011@gmail.com

The boson Hamiltonian H_{IBM} is based on the shell model, but the parameters of H_{IBM} are determined phenomenologically, based on the energy level data and on some specific $B(E2)$ values as input. The computer program PHINT of Scholten [12] is used to set up the Hamiltonian H_{IBM}. Its solution yields the eigenvalues and eigenfunctions. The absolute $B(E2)$ values and $B(E2)$ ratios are also deduced.

B. Dynamic pairing plus quadrupole (DPPQ) model

The microscopic theory of collective motion in nuclei is based on the shell model. In the dynamic pairing plus quadrupole model of Kumar and Baranger [10,11], for the residual nucleon-nucleon interaction, it employs the long range quadrupole interaction and the short range pairing interaction. The H_{PPQ} is built on the spherical single-particle basis, to which the quadrupole and pairing interaction terms are added on equal footing in the generalized Bogoliubov transformation (GBT) method [10,11]. The two valence shells with ($n = 4, 5$) for protons and ($n = 5, 6$) for neutrons were employed [10,11],

$$H_{PPQ} = H_s + H_Q + H_P. \qquad (3)$$

The seven parameters of the five-dimensional collective Hamiltonian H_{coll} are determined microscopically from the solution of H_{PPQ}. No input data of level energies or $B(E2)$ values are required as input. Slight variation of the quadrupole force strength $\chi = X \times A^{-1.4}$ (MeV) is allowed to approximately reproduce the energy scale in $E(2_1^+)$. Also the ($Z = 40, N = 70$) inert core effect is taken into account through the mass renormalization factor F_B, which multiplies all the six inertial coefficients in T_{vib} and T_{rot} [Eq. (4)],

$$H_{coll} = V(\beta, \gamma) + T_{vib}(\beta, \gamma) + T_{rot}(\beta, \gamma). \qquad (4)$$

A two-dimensional triangular array of (β, γ) points is set up, and the Hamiltonian is solved for each of the 92 points of the triangular array. A summation over the (β, γ) array yields the final values of the properties of the nucleus. See Refs. [10,11] for more details. For the mass region with ($N < 82$) nuclei, the inert core of ($Z = 40, N = 40$) was employed by Gupta and Kumar (2012) [13] for the study of ($N = 72$–78) $^{130-136}$Ce isotopes. The same inert core is also employed for the present study of ($N = 66$–72) Te isotopes.

III. RESULTS

A. Ground band

The ground band level energies (NNDCs) [14] of up to spin $I^\pi = 6^+$, for $A = 118$–128 Te isotopes are depicted in Fig. 1. At $A = 120$, the energy of the 2_1^+ state is minimum (~560 keV), and rises up to about 603 keV in ^{124}Te. That means a variation of 43 keV or ~7% only up to $N = 72$, with sharper rise at higher $N = 74, 76$ ^{126,128}Te. The intraband equal level energy spacing corresponds to the spherical anharmonic vibrator pattern. The anharmonicity may be defined in terms of the deviation of the energy ratio $R_{4/2} = E(4^+)/E(2_1^+)$ value from the value of 2.0 for the harmonic vibrator.
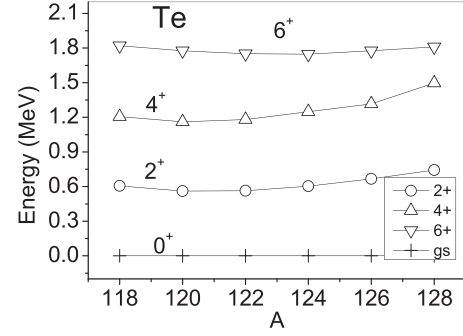

FIG. 1. Plot of ground band (partial) spectrum of $^{118-128}$Te isotopes.

The energy ratio $R_{4/2} = E(4_1^+)/E(2_1^+)$ provides a good measure of the shape of a nucleus. As is well known, it is equal to 2.0 for spherical harmonic vibrator, 2.2 for an E(5) nucleus [15], 2.5 for the γ-unstable triaxial rotor [16] or O(6), 2.92 for an X(5) nucleus [17], and 3.33 for the deformed rotor [18]. A maximum value of $R_{4/2}$ of 2.09 at $A = 122$ is obtained in $^{118-124}$Te isotopes (Fig. 2). Other more neutron rich or neutron deficient Te isotopes have lesser values of $R_{4/2}$. Thus, the energy spectra of the ground bands in Te isotopes display the spherical anharmonic vibrational character.

The single term power index formula,

$$E(I) = a I^{b}, \qquad (5)$$

proposed by Gupta *et al.* (1995) [19] for ground band level energies, provides statewise deformation status of the nucleus. If the level structure is stable, a horizontal plot of the power index "$b(I)$" versus spin I is obtained. Here ^{118,120}Te, with ground band extending up to spin $I^\pi = 12^+$, exhibit (Fig. 3) constancy up to spin 6^+, and a sharp rise for the higher spins, signifying a change in the ground band structure, which may be due to the change in shape deformation. For the $N = 70, 72$ ^{122,124}Te, the ground band terminates at spin $I^\pi = 6^+$ [14]. The shape phase transition at spins higher than 6^+ can be associated with the shape coexistence.

In a recent survey of the shape coexistence phenomenon, Bonatsos *et al.* [20] suggested its presence in $A = 116, 118, 120$ Te isotopes, and suggested it due to the particle hole excitation of the valence proton induced by the valence neutrons at
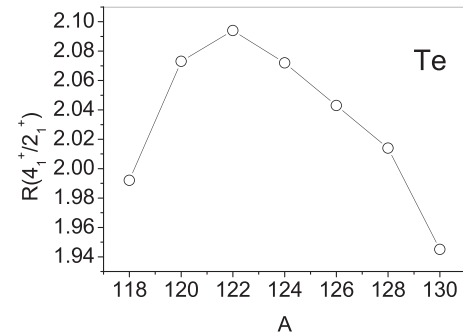

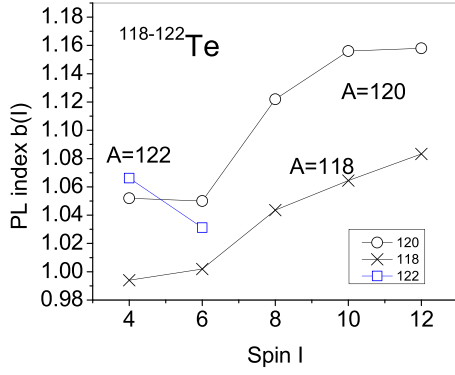FIG. 2. Plot of energy ratio $R_{4/2}$ in $^{118-130}$Te isotopes.

FIG. 3. Plot of power index "$b(I)$" for $N = 66, 68, 70$ $^{118-122}$Te.

the midshell. That may occur here at the higher spin at higher level energy.

The occurrence of this phenomenon in the nuclei near the proton magic number is due to the proximity of $h_{11/2}$ neutron orbits to the Fermi surface at the small ground state deformation. The p-n interaction of the $g_{9/2}$ proton orbit and the $h_{11/2}$ neutron orbit may enhance this effect. At higher spin, the neutrons may get up into the $h_{11/2}$ orbits from the lower $g_{7/2}$ and $d_{5/2}$ neutron orbits, inducing increased deformation at higher spins.

It is interesting to look at the correlation of the reduced $E2$ transition probability $B(E2, 0_1^+ - 2_1^+) = B(E2) \uparrow$ [21] versus the energy inverse $[1/E(2_1^+)]$ related to the kinetic moment of inertia of the given nucleus. A linear relation is exhibited between the two entities (Fig. 4) [22] for $A = 120$–128 Te isotopes. However, the finite value of $B(E2) \uparrow$ of $0.70e^2b^2$ at $A = 120$, is relatively large for a low energy ratio $R_{4/2}$ of less than 2.1 and hence it may be considered as an indicator of the dynamic deformation features of the anharmonic vibrator nucleus ^{120}Te. Also, the maximum occurs at $N = 68$ ^{120}Te rather than at $N = 66$ ^{118}Te, the midpoint of the $N = 50$–82 shell space, or at $N = 70$ ^{122}Te, with the maximum $R_{4/2}$ energy ratio. That signifies the more deformed status of ^{120}Te, as further illustrated below from its potential energy surface (PES). The occurrence of the maximum deformation features at $N = 66, 68, 70$ $^{118-122}$Te illustrates the effects of the neutrons filling in the Nilsson single particle orbits of the
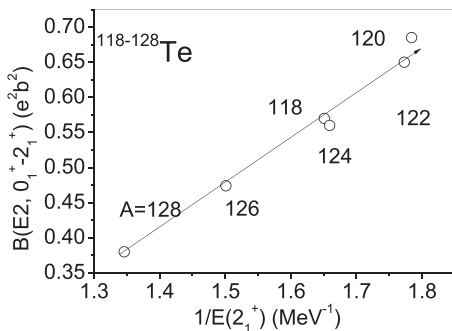

FIG. 4. Plot of $B(E2, 0_1^+ - 2_1^+)$ $(e^2 b^2)$ versus $[1/E(2_1^+)]$ (MeV^{-1}) for $^{118-128}$Te isotopes.
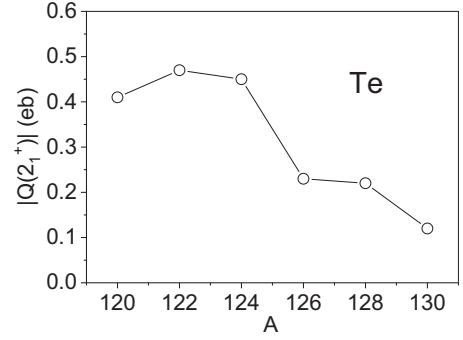

FIG. 5. Quadrupole moment $Q(2_1^+)$ (eb) $(-ve)$ versus atomic mass number A for Te isotopes.

$\nu h_{1/2}$ subshell, beyond the $\nu d_{5/2}$ and $\nu g_{7/2}$ subshells [18] (see Fig. 19 below).

The electric quadrupole moment is of negative sign, and $|Q(2_1^+)|$ is increasing with increasing neutron hole pairs (from $N = 78, A = 130$) (decreasing A) and is maximum at $N = 70$ ^{122}Te (Fig. 5). The data are taken from the compilation of Bokish *et al.* [4]. The value for ^{120}Te is estimated to be about $-0.40eb$, based upon the $E2$ matrix element [2]. It is well known [11] that even for the spherical vibrator, on account of the anharmonicity a finite quadrupole moment and $B(E2, 0_1^+ - 2_1^+)$ is possible, which of course indicates the deformation component in the vibration. Larsen *et al.* [23] ascribed this property of the anharmonic vibrators to the effect of the mixing of the two phonon states into the one phonon state. As will be shown below, the nonzero quadrupole moment is also predicted in the present IBM and DPPQ model calculation. This resolves the dichotomy pointed out above in Ref. [2].

It is worth noting that the asymmetry parameter γ is more than 20° for the γ-unstable rotors [16]. Also, for the spherical vibrator γ lies between 20° and 30°, so that from the values of γ alone one may not be able to distinguish between the two views.

Figures 1, 2, 4, and 5 for the ground band indicate decreasing deformation of Te isotopes with increasing N, because of the decreasing number of hole pairs. The study of the excited vibrational multiplets indicates the anharmonic vibrator status of the Te isotopes.

B. Excited phonon multipets in Te

The $n = 2$ phonon triplet energy spectrum of $A = 118$–128 Te isotopes is displayed in Fig. 6. While the $n = 1$ phonon singlet energy of the spin $I^\pi = 2_1^+$ state varies slowly from a minimum of 560 keV in ^{120}Te to 603 keV up to ^{124}Te and up to 742 in $A = 128$ Te, the energy of the excited $I^\pi = 0_2^+$ state of the $n = 2$ triplet varies sharply from 557 keV at ^{118}Te to 1979 keV in ^{128}Te.
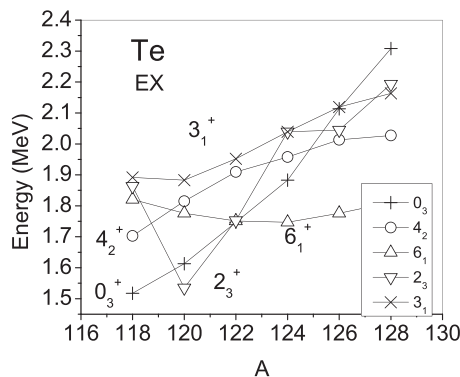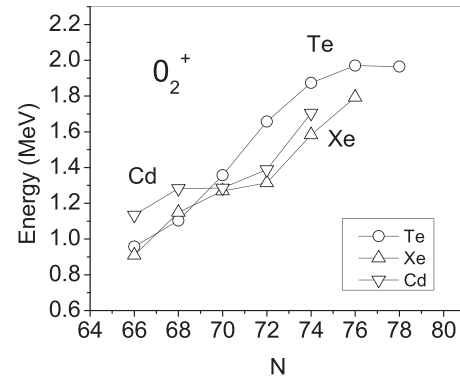
The state energies $E(4_1^+)$ and $E(2_2^+)$ increase smoothly with increasing mass number A, in consonance with the 2_1^+ state. In the $n = 2$ triplet, the 2_2^+ state (cross symbol) rises above the 4_1^+ state (open square) at ^{120}Te, and the two states rise together. This smooth variation with mass number A is
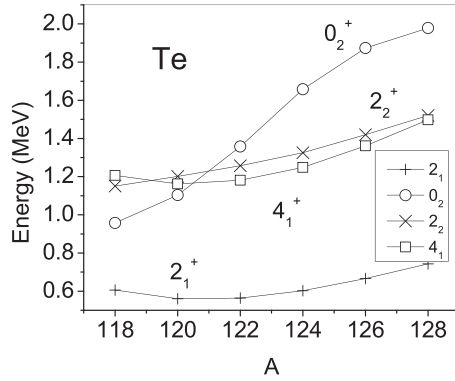
FIG. 6. Plot of $n = 2$ triplet spectrum in $A = 118$–128 Te.

FIG. 8. Variation of $E(0_2^+)$ of the $n = 2$ triplet versus N in Te, Cd, and Xe.

interesting. Note that both $R_{4/2}$ and QM $|Q(2_1^+)|$ decrease with increasing A.

As stated above, Robinson *et al.* [5] associated the spectrum of ^{124}Te with the O(6) symmetry of IBM [6], on account of the high lying 0_2^+ state. However, the Te isotopes have an energy ratio $R_{4/2}$ less than 2.1, and thus lie below the E(5) critical point symmetry, with $R_{4/2}$ of 2.2. Later, Hicks *et al.* [8] associated ^{124}Te with the E(5) critical point symmetry, which is associated with flat square potential of infinite depth, which is not applicable to the Te isotopes. A continuous rise of the state 0_2^+ in Te isotopes needs a more general view of the special features in the anharmonic vibrator view. Also one needs to take into account the $n = 3$ quintuplet (Fig. 7), wherein the 0_3^+ state follows the rise of the 0_2^+ state, unlike their relation in the E(5) critical point symmetry [15].

The $n = 3$ quintuplet spectra of the Te isotopes are displayed in Fig. 7. In the ground bands, the 6_1^+ state falls down up to ^{122}Te, and then rises up for the higher mass number A. That indicates the changing nuclear anharmonicity at the higher mass. The state 0_3^+ (plus symbol) rises up sharply with increasing A, as seen for the 0_2^+ state (Fig. 6). The 4_2^+ and 3_1^+ states rise up together with increasing A. But the movement of the 2_3^+ state is more varied. In ^{118}Te, it lies high, and in ^{120}Te it lies the lowest, forming a part of the close lying levels of the quintuplet. Also note that the 4_2^+ state lies below the 3_1^+ state for all A, opposite to the order in the rotor

model. The rise of excited 0^+ states is correlated with the occupation of the up-sloping Nilsson orbit of $d_{5/2}$ and $h_{11/2}$ (Fig. 19).

It is of general interest to further understand the sharp rise of the 0_2^+ state, with increasing A or N. The variation of $E(0_2^+)$ with N for Te, along with Xe and Cd is depicted in Fig. 8. All of them show an almost similar rise with N. The energy ratio $R_{4/2}$ decreases with increase of N in $N = 66$–78 region in each of them. On the microscopic level, it is related to the variation of the single particle Nilsson orbits, with increasing filling of the up sloping orbits. But the rise of 0_2^+ faster than 4_1^+ and 2_2^+ states indicates the greater saturation of the β degree of freedom for the axially symmetric vibration. The Te curve lies higher than the Xe curve, indicating a larger effective saturation effect in Te. Also see its reproduction in theory (see Fig. 12, below). A similar rise of the 0_3^+ state of the $n = 3$ quintuplet is observed for Te, Xe, and Cd (Fig. 9).

C. Theoretical results

The interacting boson model and the microscopic DPPQ model are used to study the band structure and the intraband and intermultiplet $B(E2)$ values and $B(E2)$ ratios, limited to $A = 118$–124 Te, which are of relatively more stable shape. In Table I, the IBM parameters of Eq. (2) are listed for the four Te isotopes. Also the quadrupole strength parameter X and the

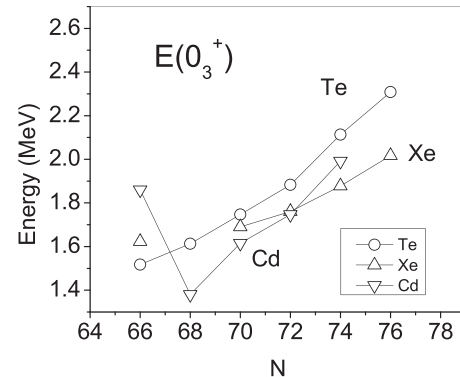FIG. 7. Plot of quintuplet energy spectrum of $A = 118$–128 Te.

FIG. 9. Variation of $E(0_3^+)$ versus N in Te, Cd, and Xe.

TABLE I. IBM-1 parameters (keV) for Te isotopes, in PHINT notation, and of the DPPQ model. The PHINT parameters EPS, QQ, ELL, and PAIR are related to the coefficients ε, k, k', and k'' of Eq. (2), respectively.

A	EPS	QQ	ELL	PAIR	X	F_B
118	758.1	−21.8	3.5	11.4	68.0	2.4
120	658.1	−16.6	8.1	2.00	69.0	2.2
122	727.7	−20.0	1.3	11.6	70.0	2.4
124	855.9	−21.0	4.6	34.5	71.0	2.6

inertial factor F_B of the DPPQ model are listed for the four Te isotopes.

As stated above, the parameters used for the IBM-1 calculation, using the PHINT computer program of Scholten [12], are listed in Table I. The phonon energy parameter EPS ($=\varepsilon$), and the quadrupole term coefficient QQ [related to k, in Eq. (2)] vary by a small amount. The small variation in the energy terms reflects the almost uniform vibrational energy of the ground band and the two and three phonon multiplets. Their variation with mass number A is illustrated in Figs. 10 and 11. A similar pattern of the two terms is apparent. The angular momentum term coefficient k' (ELL) and the pairing term coefficient k'' (PAIR) vary by larger amounts. These terms reflect the variations in the order of spins in the phonon mutiplets with neutron number N.

The solutions of the IBM Hamiltonian, with the coefficients of the various terms of H_{IBM} fitted to the input energy level data, are listed in Table II, and compared with the experimental values (NNDC) [14]. While some spin levels lie close to experiment, others differ by larger amounts. As illustrated below in the figures, the basic patterns of the one phonon singlet and the two and three phonon multiplets correspond to experiment in all cases.

For a quick view, the variation of the energy of the 0_2^+ and 0_3^+ in experiment are compared with the predictions in the IBM and the DPPQ models in Figs. 12 and 13. The variation of $E(0_2^+)$ with atomic number A is well reproduced in theory. Note that in the DPPQ model no input energy level data are
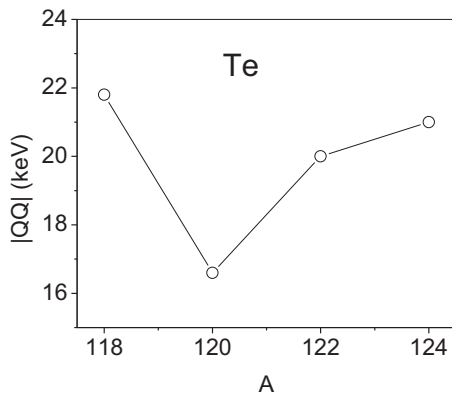

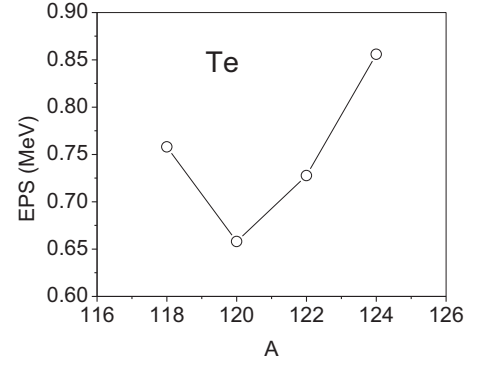FIG. 10. Plot of quadrupole interaction term coefficient $|QQ|$ ($= 2k$) in IBM.

FIG.11. Plot of boson energy term coefficient ε (EPS) in IBM.

used, so that the reproduction of variation of 0_2^+ with A in the microscopic approach reflects the effect of the Nilsson single particle orbits, and indicates the effect of the nuclear rigidity with increasing A in the Te isotopes.

The variation of $E(0_3^+)$ with A is also reproduced in IBM. However, in the DPPQ model the predicted energies lie higher. The DPPQ model also predicts a PES minimum at $\beta_0 = 0.174$ for $^{118-122}$Te and 0.13 for ^{124}Te. Thus it supports the weak deformation for the $^{118-122}$Te and less for heavier Te.

D. Comparison of level spectra in Te with theory

The partial energy spectra for ^{118,120,122,124}Te are given in Figs. 14–17, illustrating the formation of the $n = 2$ phonon triplet and $n = 3$ phonon quintuplet, along with the predictions from theory (IBM-1 and DPPQ model). The basic pattern of the anharmonic phonon multiplets are reproduced in the IBM-1 and DPPQ models. In ^{118}Te, the quintuplet in the DPPQ model lies higher and its split is somewhat larger. In the heavier Te isotopes, the reproduction of triplet and quintuplet is better (Figs. 15–17) in the DPPQ model.

TABLE II. Level energies (keV) in EX and theory for Te.

| Spin	2_1^+	4_1^+	2_2^+	0_2^+	6_1^+	4_2^+	3_1^+	2_3^+	0_3^+
^{118}Te									
EX	606	1206	1151	958	1821	1703	1892	1863	1517
IBM-1	490	1051	1152	1069	1689	1810	1802	1747	1912
DPPQ	511	1022	1496	1111	1591	2215	2347	1997	2554
^{120}Te									
EX	560	1162	1201	1103	1776	1815	1863	1535	1613
IBM-1	584	1221	1215	1098	1918	1897	1880	1744	1870
DPPQ	538	1082	1477	1167	1681	2205	2318	2006	2576
^{122}Te									
EX	564	1181	1257	1357	1751	1910	1952	1753	1747
IBM-1	552	1157	1216	1192	1819	1895	1896	1889	1963
DPPQ	560	1147	1353	1284	1785	2061	2121	2050	2465
^{124}Te									
EX	603	1249	1326	1657	1747	1958	2039.3	2039.4	1883
IBM-1	627	1352	1380	1516	2168	2196	2178	2375	2232
DPPQ	637	1335	1375	1583	2110	2149	2139	2480	2335
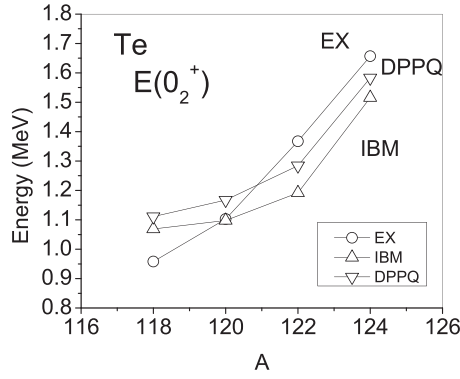
FIG. 12. Variation of $n = 2$ excited 0_2^+ state in Te in theory.
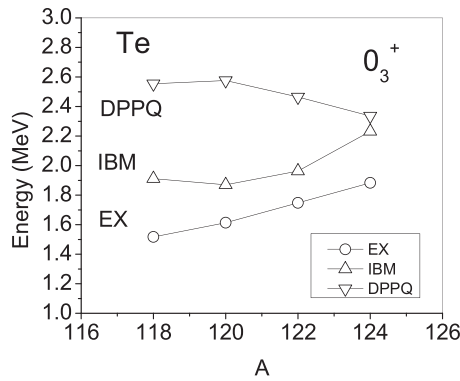
FIG.13. Variation of $n = 3$ excited 0_3^+ state in Te in theory.
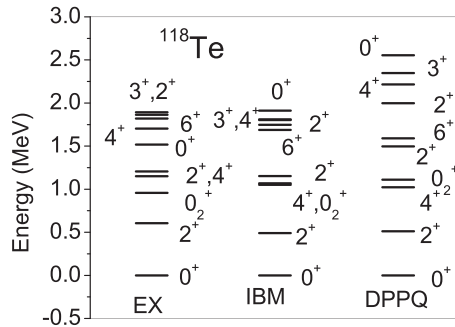
FIG. 14. Comparison of IBM and DPPQ model results with EX for ^{118}Te.
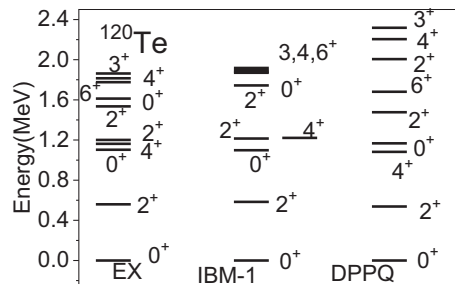
FIG. 15. Comparison of IBM-1 and DPPQ model results with EX for ^{120}Te.
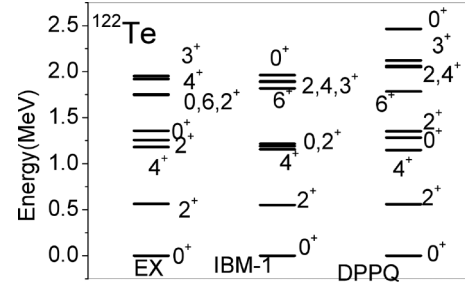
FIG. 16. Energy spectrum (partial) of ^{122}Te in EX and theory.

The occupation of the Nilsson single particle orbits in the even A Te isotopes can also be estimated from the study of the spectra in the neighboring odd-A isotopes. These spectra for $N = 65, 67, 69, 71$, $A = 117$–123 Te isotopes are illustrated in Fig. 18, as listed in NNDC [14]. The ground state spin is $\frac{1}{2}^+$ in all cases. Above the $N = 50$ closed shell, the orbits in the neutron subshells of $d_{5/2}$, $g_{7/2}$, and $h_{11/2}$ (Fig. 19) may be filled. At small deformation of $\beta = 0.1$ in Te, the four orbits of $g_{7/2}$ and three of $d_{5/2}$ may be occupied by 14 valence neutrons. There after the $[550 \frac{1}{2}]$ orbit of the $h_{11/2}$ sub shell may be occupied at higher energies.

E. The E2 transitions in Te

According to the U(5) symmetry rules for $B(E2)$ ratios, the ratio $B(E2, 4_1^+ - 2_1^+)/B(E2, 2_1^+ - 0_1^+)$ is 2.0 and $B(E2, 6_1^+ - 4_1^+)/B(E2, 2_1^+ - 0_1^+)$ is 3.0. For increasing anharmonicity, the values for the $B(E2)$ ratios are reduced. From the Coulomb excitation experiment, absolute $B(E2)$ values and QM $Q(2_1^+)$ are compared with the IBM-1 and DPPQ models for ^{118}Te in Table III and for ^{120}Te in Table IV. The basic pattern is obtained in experiment, as well as in theory (IBM and DPPQ models). The $\Delta n = 1$ strong $B(E2, 2_2^+ - 2_1^+)$ transition and weak $\Delta n = 2$ $B(E2, 2_2^+ - 0_1^+)$ transition is predicted in theory. The $B(E2, 2_2^+ - 2_1^+)/B(E2, 2_1^+ - 0_1^+)$ ratio is ~1.5 for ^{120}Te in IBM, but is reduced in the DPPQ model. The nonzero (negative) value of the quadrupole moment $Q(2_1^+)$ is also predicted for the two isotopes. That resolves the dichotomy referred to above.

In NNDC compilation [14], 1482 and 1863 keV are listed as $(1, 2)^+$. Here the latter as the 2_3^+ state is adopted in Table V. But in both alternatives, its decay to the 0_2^+ state is not according to expectation of phonon rules.
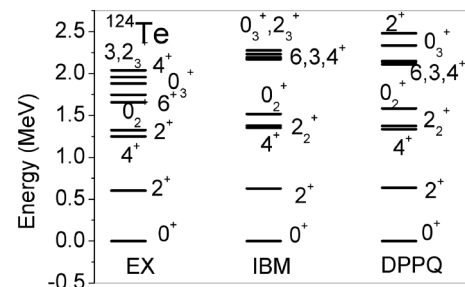
FIG. 17. Energy level spectrum (partial) of ^{124}Te in EX and theory.
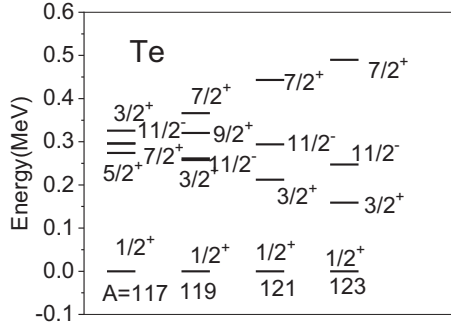
FIG.18. Energy level spectra of $^{117-123}$Te isotopes.

The $B(E2)$ ratios in experiment are compared with the IBM-1 and IBM-2 [2] and DPPQ models [11] for members of the two and three phonon multiplets in Table VI. for ^{120}Te.

The $B(E2,2_2 - 2_1^+)/B(E2,2_2^+ - 0_1^+)$ $\Delta n = 1/\Delta n = 2$ ratio is large. The wide variation in Coulomb excitation [2,3] and the one derived from I_γ, E_γ [14] and also in theory (IBM, DPPQ) arises on account of the very small value of the denominator, which varies through the large factor.

The $B(E2)$ ratios for the $E2$ transitions from the 2_3^+ state of the quintuplet to states 2_2^+ and 0_2^+ are almost equal, as also given approximately in theory. The values for $\Delta n = 2$ $E2$ transition to the 2_1^+ state are as expected. Similar agreement also occurs for the $E2$ transitions from 3_1^+ and 4_2^+ states.

The absolute $B(E2)$ values [21] for $N = 70, 72$ ^{122,124}Te are exhibited in Table VII. The absolute values and the variation with N or A are easily obtained from theory. The quadrupole moment values [4] for ^{122}Te and ^{124}Te also compare well with theory.

For ^{122,124}Te, the intermultiplet $B(E2)$ ratios are listed in Tables VIII and IX. The $B(E2)$ ratios for $E2$ transitions from the 2_3^+ state of the quintuplet to the states 2_2^+ and 0_2^+ of the triplet are large in ^{122}Te, as also given in theory. The value for $\Delta n = 2$ $E2$ transition to the 2_1^+ state is small, as expected. For the 3_1^+ state, the smaller $B(E2)$ to 2_1^+ and larger $B(E2)$ to 4_1^+ and 2_2^+ states of the triplet are also predicted in theory. Similarly, the $B(E2)$ from 4_3^+ of the $n = 2$ quintuplet, large for transitions to 4_1^+ and 2_2^+ of the triplet states, are well predicted. Thus the $E2$ transitions between the quintuplet and triplet states in experiment are predicted fairly well in theory.
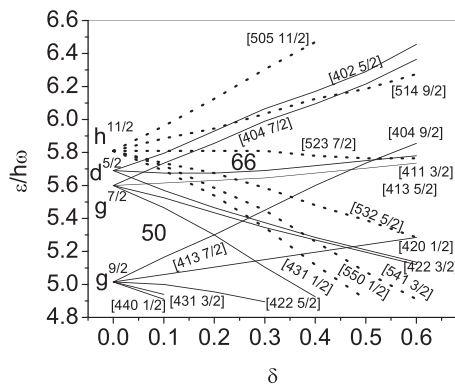
FIG. 19. Nilsson single particle orbits above $N, Z = 50$.

TABLE III. Absolute $B(E2)$ ($e^2 b^2$) and QM (eb) for ^{118}Te.

Isotope	EX [21,24]	IBM	DPPQ
$B(E2, 2_1^+ - 0_1^+)$	0.114 (22)	0.218	0.137
$B(E2 4_1^+ - 2_1^+)$		0.37	0.274
$Q(2_1^+)$ eb		−0.60	−0.73
$B(E2, 2_2^+ - 2_1^+)$	0.55 (28)	0.26	0.092
$B(E2, 2_2^+ - 0_1^+)$	0.0036 (15)	0.0065	0.0076

IV. POTENTIAL ENRGY SURFACE (PES)

In Fig. 20 a plot of the potential energy surface $V(\beta, \gamma = 0°)$, as predicted in the microscopic DPPQ model, is exhibited. The potential minimum lies on the prolate edge but is shallow, and is wiped out at the zero point energy of the ground state, indicating an anharmonic vibrator shape for ^{120}Te.

In Fig. 21, the full PES $V(\beta,\gamma)$ is depicted. It clearly demonstrates the prolate deformation for ^{120}Te, but the contours seem to correspond to the γ-independent vibration. The PES plot clearly demonstrates the $\gamma_{\rm RMS} \sim 30°$ value for the near spherical vibrator. The triaxiality in an almost spherical vibrator nucleus like Te is not the same as the triaxiality of a rigid rotor. However, the rigid rotor expression of $R_\gamma = E(2_\gamma)/E(2_{\rm g})$ does yield the value of γ equivalent to $\gamma_{\rm RMS}$.

V. SUMMARY AND DISCUSSION

The energy level spacing in the ground state band up to spin 6^+ for $N = 68-78$ $^{118-128}$Te, are exhibited, along with the energy ratio $R_{4/2}$ (Figs. 1 and 2), which clearly indicates the vibrational anharmonicity in the Te isotopes. The power law index "$b(I)$" up to 6^+ in $^{118, 120}$Te are constant and small (Fig. 3). The sharp increase at higher spin indicates the occurrence of a shape phase transition at higher spin. It is an example of the shape coexistence in nuclei close to the magic numbers, as cited in Ref. [20]. Also, at larger spins, the neutrons may move up from the lower orbits to the $h_{11/2}$ orbits, leading to increased deformed spectrum.

The linear plot of $B(E2, 0_1^+ - 2_1^+)$ versus $[1/E(2_1^+)]$ (Fig. 4) indicates the maximum at $N = 68$ ($A = 120$), and a regular fall with increasing N. The plot (Fig. 5) of quadrupole moment with a maximum of $|Q(2_1^+)|$ in $N = 66, 68, 70, 72$ $^{118-124}$Te displays the anharmonicity in Te isotopes. The same is predicted in the IBM and DPPQ models. The nonzero potential minimum PES also supports the anharmonicity, leading to a nonzero quadrupole moment. Mixing of the two

TABLE IV. Absolute $B(E2)$ ($e^2 b^2$) and QM (eb) for ^{120}Te.

Isotope	EX [2]	IBM	DPPQ
$B(E2, 2_1^+ - 0_1^+)$	0.121 (4)	0.151	0.137
$B(E2, 4_1^+ - 2_1^+)$	0.200 (6)	0.265	0.270
$Q(2_1^+)$ eb	−0.41 (3)	−0.35	−0.69
$B(E2, 2_2^+ - 2_1^+)$	0.183 (9)	0.228	0.110
$B(E2, 2_2^+ - 0_1^+)$	0.0052 (8)	0.0023	0.0078

TABLE V. $B(E2)$ ratios in $N = 66$ ^{118}Te. $B(E2, I_i^+ - I_f^+)/B(E2, I_i^+ - I_{f''}^+)$ is written as $B(E2, I_i^+ - I_f^+/I_{f''}^+)$ in the first column of all the rows of this and the following tables.

$B(E2)$ ratio	EX [14]	IBM	DPPQ
$B(E2, 2_2^+ - 2_1^+/0_1^+)$	73 (7)	40	12.1
$B(E2, 2_3^+ - 0_2^+/2_1^+)$	0.61 (20)	168	8.8
$B(E2, 2_3^+ - 2_2^+/2_1^+)$	3.7 (7)	78	20.6
$B(E2, 3_1^+ - 2_1^+/4_1^+)$	0.047 (12)	0.12	0.56
$B(E2, 3_1^+ - 2_2^+/2_1^+)$	46 (12)	26	3.7
$B(E2, 4_2^+ - 2_1^+/4_1^+)$	0.008 (2)	0.019	0.064
$B(E2, 4_2^+ - 2_2^+/4_1^+)$	1.12 (22)	1.54	3.73
$B(E2, 4_1^+ - 2_1^+)/$ $B(E2, 2_1^+ - 0_1^+)$		1.71	2.00
$B(E2, 6_1^+ - 4_1^+)/$ $B(E2, 2_1^+ - 0_1^+)$		2.11	2.72

TABLE IX. $B(E2)$ ratios in $N = 72$ ^{124}Te.

$B(E2)$ ratio	EX [14]	IBM-1	DPPQ
$B(E2, 2_2^+ - 2_1^+/0_1^+)$	129 (3)	94	89
$B(E2, 2_3^+ - 0_1^+/2_1^+)$	0.100 (2)		0.082
$B(E2, 2_3^+ - 0_2^+/2_2^+)$	9.7 (60)	3.5	3.2
$B(E2, 2_3^+ - 2_2^+/4_1^+)$	1.7 (15)	0.6	2.14
$B(E2, 3_1^+ - 2_1^+/4_1^+)$	0.087 (9)	0.030	0.052
$B(E2, 3_1^+ - 2_2^+/2_1^+)$	61 (4)	102	61
$B(E2, 4_2^+ - 2_1^+/4_1^+)$	0.031 (3)	0.004	0.018
$B(E2, 4_2^+ - 2_2^+/2_1^+)$	44	289	71
$B(E2, 4_1^+ - 2_1^+)/B(E2, 2_1^+ - 0_1^+)$	1.16 (5)	1.55	1.7
$B(E2, 6_1^+ - 4_1^+)/B(E2, 2_1^+ - 0_1^+)$		1.74	2.46

TABLE VI. $B(E2)$ ratios in $N = 68$ ^{120}Te.

$B(E2)$ ratio	EX [14]	IBM-1	DPPQ	IBM-2
$B(E2, 2_2^+ - 2_1^+/0_1^+)$	86 (15) [14] 35 [2]	99	14	105
$B(E2, 2_3^+ - 0_1^+/2_1^+)$	0.112 (20)	<0.04	0.20	<0.001
$B(E2, 2_3^+ - 0_2^+/2_1^+)$	12.6 (40)	106	15	160
$B(E2, 2_3^+ - 2_2^+/2_1^+)$	11.5 (30)	51	25	28.6
$B(E2, 3_1^+ - 2_1^+/4_1^+)$	0.11 (4)	0.046	0.46	0.036
$B(E2, 3_1^+ - 2_2^+/2_1^+)$	33.6 (6)	32	8.6	65
$B(E2, 4_2^+ - 2_1^+/4_1^+)$	0.012 (3)	0.014	0.07	0
$B(E2, 4_2^+ - 2_2^+/4_1^+)$	1.2 (5)	1.3	3.11	1.096
$B(E2, 4_1^+ - 2_1^+)/$ $B(E2, 2_1^+ - 0_1^+)$	1.67 (5)	1.75	1.97	
$B(E2, 6_1^+ - 4_1^+)/$ $B(E2, 2_1^+ - 0_1^+)$		2.23	2.69	

TABLE VII. $B(E2, 2_1^+ - 0_1^+)$ $(e^2 b^2)$ and QM (eb) for $A = 122,124$ Te.

Isotope		EX [21,4]	IBM	DPPQ
$B(E2)$	^{122}Te	0.132 (2)	0.149	0.124
	^{124}Te	0.114 (2)	0.133	0.103
QM	^{122}Te	−0.47 (5)	−0.38	−0.525
	^{124}Te	−0.45 (10)	−0.32	−0.275

TABLE VIII. $B(E2)$ ratios in $N = 70$ ^{122}Te.

$B(E2)$ ratio	EX [14]	IBM-1	DPPQ
$B(E2, 2_2^+ - 2_1^+/0_1^+)$	98 (7)	88	28
$B(E2, 2_3^+ - 0_1^+/2_1^+)$	0.27 (4)	<0.17	0.25
$B(E2, 2_3^+ - 0_2^+/2_1^+)$	34 (5)	390	100
$B(E2, 2_3^+ - 2_2^+/2_1^+)$	11 (2)	153	37
$B(E2, 3_1^+ - 2_1^+/4_1^+)$	0.060 (4)	0.051	0.22
$B(E2, 3_1^+ - 2_2^+/2_1^+)$	93 (5)	56	18
$B(E2, 4_2^+ - 2_1^+/4_1^+)$	0.034 (3)	0.011	0.061
$B(E2, 4_2^+ - 2_2^+/4_1^+)$	0.46 (5)	1.3	1.9
$B(E2, 4_1^+ - 2_1^+)/B(E2, 2_1^+ - 0_1^+)$		1.66	1.85
$B(E2, 6_1^+ - 4_1^+)/B(E2, 2_1^+ - 0_1^+)$		1.98	2.58

phonons into one phonon is also suggested. That resolves the dichotomy of nonzero QM in a near magic nucleus. The variation of the two phonon triplet (Fig. 6) and the three phonon quintuplet (Fig. 7) is exhibited.

The variations of the IBM parameters are listed in Table I, and illustrated in Figs. 8 and 9. The eigenenergies of the four isotopes of Te are listed in Table II. In Figs. 10 and 11 the sharp variation of the 0_2^+ state of the two phonon triplet and of the 0_3^+ state of the $n = 3$ phonon quintuplet in Te are compared with those of Cd and Xe. A comparison of theory with experiment for the rise of the 0_2^+ state is illustrated in Figs. 12 and 13. In Figs. 14–17, comparison of the IBM-1 and DPPQ model predictions of the Te spectra with experiment is given. The spectra of odd A Te isotopes are depicted in Fig. 18, to illustrate the single particle orbit occupation of the Nilsson orbits (Fig. 19). The potential energy surface $V(\beta,\gamma)$ is displayed in Figs. 20 and 21, which illustrates the weak quadrupole deformation of $N = 68$ ^{120}Te. The zero point energy exceeds the shallow potential minimum, which leads to the anharmonic vibrator status. The two valence protons in Te leads to a nonzero potential minimum. That again resolves the dichotomy cited above, as referred to in Refs. [2,3]. The absolute $B(E2)$ values and the intermultiplet $B(E2)$ ratios are displayed in the tables in comparison with theory.
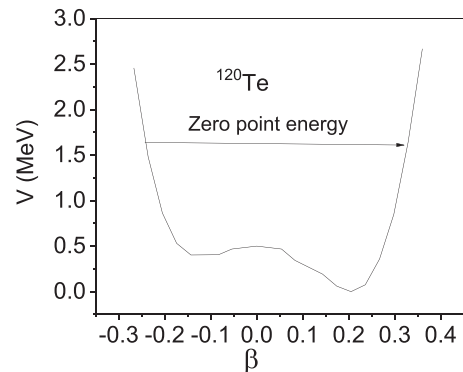

FIG. 20. Plot of $V(\beta, \gamma = 0°)$ for ^{120}Te from DPPQ model.
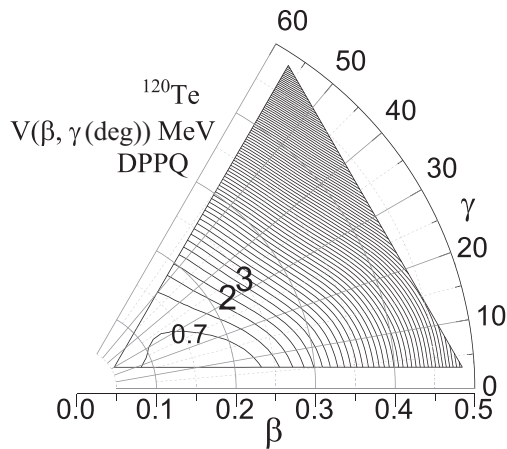
FIG. 21. Plot of $V(\beta, \gamma)$ (PES) for ^{120}Te from DPPQ model.

The yrast band energies manifest the angular momentum projections of the intrinsic spherical vibrator nuclear core and the $K^{\pi} = 2^+$ band level energies represent those of the excited vibrator. The sharp rise of the 0_2^+ and 0_3^+ state energies of Te, in common with Cd and Xe, represent the axially symmetric vibration, which requires larger energy with increasing saturation of the spherical shape. The finite $B(E2)$ and quadrupole moment further support the collective status of the Te spectra. The empirical features and the IBM and DPPQ models reproduce these basic features in Te isotopes.

ACKNOWLEDGMENT

[1] J. Barrette, M. Barrette, R. Haroutunian, G. Lamoureux, and S. Monaro, Phys. Rev. C **10**, 1166 (1974).

[2] Mansi Saxena *et al.*, Phys. Rev. C **90**, 024316 (2014).

[3] Mansi Saxena *et al.*, Acta Phys. Pol. B **49**, 541 (2018).

[4] A. Bockish and A. M. Kleinfeld, Nucl. Phys. A, **261**, 498 (1976).

[5] S. J. Robinson, W. D. Hamilton, and D. M. Snelling, J. Phys. G: Nucl. Phys. **9**, L71 (1983).

[6] F. Iachello and A. Arima, *The Interacting Boson Model* (Cambridge University Press, Cambridge, England, 1987).

[7] A. S. Davydov and Filippov, Nucl. Phys. **8**, 237 (1958).

[8] S. F. Hicks, J. R. Vanhoy, P. G. Burkett, B. R. Champine, S. J. Etzkorn, P. E. Garrett, S. W. Yates, and M. Yeh, Phys. Rev. C **95**, 034322 (2017).

[9] S. F. Hicks *et al.*, Phys. Rev. C **105**, 024329 (2022).

[10] K. Kumar and M. Baranger, Nucl. Phys. A. **110**, 529 (1968).

[11] K. Kumar, in *The Electromagnetic Interaction in Nuclear Physics*, edited by W. D. Hamlton (North-Holland, Amsterdam, 1975), Chap. 3.

[12] O. Scholten, *The Program Package PHINT KVI- 63* (Groningen).

[13] J. B. Gupta and K. Kumar, Nucl. Phys. **A882**, 21 (2012).

[14] Brookhaven National Laboratory, Chart of Nuclides of National Nuclear Data Center, http://www.nndc.bnl.gov/ENSDF.

[15] F. Iachello, Phys. Rev. Lett. **85**, 3580 (2000).

[16] L. Wilets and M. Jean, Phys. Rev. **102**, 788 (1956).

[17] F. Iachello, Phys. Rev. Lett. **87**, 052502 (2001).

[18] A. Bohr and B. R. Mottelson, *The Nuclear Structure* (W. A. Benjamin, New York, 1975), Vol. II.

[19] J. B. Gupta, A. K. Kavathekar, and R. Sharma, Phys. Scr. **51**, 316. (1995).

[20] D. Bonatsos, K. E. Karakatsanis, A. Martinou, T. J. Mertzimekis, and N. Minkov, Phys. Rev. C **106**, 044323 (2022).

[21] B. Pritychenko, M. Birch, B. Singh, and M. Horoi, At. Data. Nucl. Data Tables **107**, 1 (2016).

[22] J. B. Gupta and Vikas Katoch, Int. J. Mod. Phys. E **27**, 1850033 (2018).

[23] R. D. Larsen, J. A. Thomson, R. G. Kerr, R. P. Sharenberg, and W. R. Lutz, Phys. Lett. **B40**, 360 (1972).

[24] J. J. van Ruyven, W. H. A. Hesselink, J. Akkermans, P. van Nes, and H. Verheul, Nucl. Phys. A **380**, 125 (1982).